Properties of the mean momentum balance in turbulent boundary layer, pipe and channel flows

By T. WEI[1], P. FIFE[2], J. KLEWICKI[1] AND P. McMURTRY[1]

[1]Department of Mechanical Engineering, University of Utah, Salt Lake City, UT 84112, USA
[2]Department of Mathematics, University of Utah, Salt Lake City, UT 84112, USA

The properties of the mean momentum balance in turbulent boundary layer, pipe and channel flows are explored both experimentally and theoretically. Available high-quality data reveal a dynamically relevant four-layer description that is a departure from the mean profile four-layer description traditionally and nearly universally ascribed to turbulent wall flows. Each of the four layers is characterized by a predominance of two of the three terms in the governing equations, and thus the mean dynamics of these four layers are unambiguously defined. The inner normalized physical extent of three of the layers exhibits significant Reynolds-number dependence. The scaling properties of these layer thicknesses are determined. Particular significance is attached to the viscous/Reynolds-stress-gradient balance layer since its thickness defines a required length scale. Multiscale analysis (necessarily incomplete) substantiates the four-layer structure in developed turbulent channel flow. In particular, the analysis verifies the existence of at least one intermediate layer, with its own characteristic scaling, between the traditional inner and outer layers. Other information is obtained, such as (i) the widths (in order of magnitude) of the four layers, (ii) a flattening of the Reynolds stress profile near its maximum, and (iii) the asymptotic increase rate of the peak value of the Reynolds stress as the Reynolds number approaches infinity. Finally, on the basis of the experimental observation that the velocity increments over two of the four layers are unbounded with increasing Reynolds number and have the same order of magnitude, there is additional theoretical evidence (outside traditional arguments) for the asymptotically logarithmic character of the mean velocity profile in two of the layers; and (in order of magnitude) the mean velocity increments across each of the four layers are determined. All of these results follow from a systematic train of reasoning, using the averaged momentum balance equation together with other minimal assumptions, such as that the mean velocity increases monotonically from the wall.

1. Introduction

Laminar to turbulent transition in boundary layer, pipe and channel flows is accompanied by dramatic redistributions of the momentum and vorticity fields, e.g. Lighthill (1963), Willmarth (1975). These redistributions, which continue to occur with increasing Reynolds number within the turbulent regime, are reflected in the shape of the mean velocity profile. Over the past decade, research regarding the mean velocity profile in turbulent wall flows has intensified, e.g. Gad-el-Hak & Bandyopadhyay (1994), Barenblatt, Chorin & Prostokishin (1997), George & Castillo (1997), Sahay (1997), Sreenivasan & Sahay (1997), Zagarola & Smits (1998), Wosnik, Castillo & George

(2000), Afzal (2001*a*, *b*), Zanoun *et al.* (2002), and Panton (2002, 2003). Despite these efforts, fundamental questions concerning the proper analytical forms of the mean velocity profiles in boundary layer, pipe and channel flows remain largely unanswered. At the heart of this matter is the fact that the equations from which the profile is derived (i.e. the time-averaged Navier–Stokes equations) are unclosed, and thus are resistive to, for example, standard perturbation methods. Apart from this, further progress requires confronting other difficult to resolve issues. These relate to both the quality of the data and the selection of appropriately sensitive, yet measurable, indicator functions employed in distinguishing between the various proposed analytical forms for the velocity profile. For example, considerable discussion has surrounded the potential effects of surface roughness on the Princeton superpipe data, Perry, Hafez & Chong (2001), while the comparison of the gradient functions, $y^+(dU^+/dy^+)$ and $(y^+/U^+)(dU^+/dy^+)$, for respectively determining logarithmic or power law forms, presents stringent demands on the data quality relative to the subtleties of the issues at hand, Wosnik *et al.* (2000).

   Given this context, it is useful to remain cognizant of the primary physical/technological motivations underlying the mean profile research efforts. Specifically, a primary (if not the primary) importance associated with determining the velocity profile lies in its inherent description of the momentum/vorticity redistribution processes mentioned at the outset. Specifically, at a practical technical level a knowledge of the mean profile translates to a predictive formula for the skin friction. More generally, turbulent wall flows are traditionally divided into four layers,

   viscous sublayer: $y^+ < 5$,
   buffer layer: $5 < y^+ < 30$,
   logarithmic layer: $30 < y^+ < 0.15\delta^+$,
   wake layer: $y^+ > 0.15\delta^+$,

where, as is customary, $+$ signifies normalization by $u_\tau = \sqrt{\tau_w/\rho}$ and ν, and δ is the boundary layer thickness or half-channel height. As is apparent, these layers are closely tied to the properties of the mean profile, and thus a more subtle influence of mean profile structure relates to the associated physical interpretations of wall-flow physics. In a pipe or channel, the flow dynamics embody the processes by which momentum is extracted from the applied mean pressure force, transported to the wall, and transmitted into a mean surface shear force. In boundary layers the processes are similar, except that the mean pressure force is replaced by mean advection. In either case, a major motivation for correctly determining the mean velocity profile is the property that it inherently, albeit indirectly, reflects these momentum transport dynamics and their scaling with Reynolds number. Since mean dynamics are described by the time-averaged momentum balance, it is rational to expect that explicit study of the mean momentum balance, and its scaling behaviours, will be of considerable utility.

   The present study employs existing high-quality data sets to reveal the properties of the mean momentum balance in boundary layer, pipe and channel flows. This analysis indicates that these turbulent wall flows are composed of a basic four-layer structure, with the dynamics in each of these layers predominantly characterized by a balance of two of the three terms in the mean momentum equation. The four-layer structure revealed is unambiguous in its connection with the relevant mean dynamics and stands in contrast to the accepted mean profile-based characterization (i.e. the sub-, buffer, logarithmic and wake layer composition mentioned above). The Reynolds number scaling properties of the momentum balance are also revealed. In doing so, clear Reynolds number dependences in the thicknesses of the four layers, as well as the velocity increments across these layers, are identified. Consistent with

this, multiscale analyses (under a minimal set of assumptions) are subsequently used to construct a new theoretical framework for turbulent channel flow. These analyses indicate that a length scale intermediate to the traditional inner and outer scales is required to properly describe mean flow structure, and thus embrace the experimental observations made herein.

2. The mean momentum balance

The streamwise mean momentum equation for fully developed channel flow is

$$0 = -\frac{1}{\rho}\frac{\mathrm{d}P}{\mathrm{d}x} + v\frac{\mathrm{d}^2 U}{\mathrm{d}y^2} - \frac{\mathrm{d}\langle uv \rangle}{\mathrm{d}y},$$

where the mean pressure gradient is

$$-\frac{\mathrm{d}P}{\mathrm{d}x} = \frac{\tau_w}{\delta},$$

and δ is the channel half-height. Normalizing the mean velocity, U, and Reynolds stress, $-\langle uv \rangle$, by the friction velocity u_τ, and y by the viscous length scale v/u_τ, gives the normalized streamwise mean momentum equation

$$0 = \frac{1}{\delta^+} + \frac{\mathrm{d}^2 U^+}{\mathrm{d}y^{+2}} - \frac{\mathrm{d}\langle uv \rangle^+}{\mathrm{d}y^+}. \tag{2.1}$$

Three physical mechanisms are represented in equation (2.1). The first term, $1/\delta^+$, is the normalized pressure gradient which provides the driving force for the flow, the second term, $\mathrm{d}^2 U^+/\mathrm{d}y^{+2}$, is the gradient of the viscous stress and the third term, $\mathrm{d}(-\langle uv \rangle^+)/\mathrm{d}y^+$, is the gradient of the Reynolds stress.

For the zero-pressure-gradient turbulent boundary layer, the inner normalized mean momentum equation is

$$U^+\frac{\partial U^+}{\partial x^+} + V^+\frac{\partial U^+}{\partial y^+} = \frac{\partial^2 U^+}{\partial y^{+2}} - \frac{\partial \langle uv \rangle^+}{\partial y^+}. \tag{2.2}$$

As in turbulent channel flow, there are three different physical mechanisms represented. Mean advection is represented by the terms on the left-hand side of equation (2.2). The other two mechanisms are the same as in channel flow: the gradient of the viscous stress, $\partial^2 U^+/\partial y^{+2}$, and the gradient of the Reynolds stress, $\partial(-\langle uv \rangle^+)/\partial y^+$.

2.1. *Force balance data*

Physically, the above momentum balance equations represent the time-average statement of Newton's second law for a differential fluid element. Examination of the mean momentum equations ((2.1) and (2.2)), indicates that it is the stress gradients (viscous, Reynolds stress, or pressure) that are the significant quantities in the force balance, not the stresses themselves. Based on the momentum equations, the three effects must all be in balance, or have two nominally in balance with the third much smaller. Therefore, for the purpose of elucidating the mean momentum transport it is useful to examine the ratio of the gradient of the viscous stress to the gradient of the Reynolds stress. If, for example, this ratio in a pipe is

$$\left| \mu\frac{\partial^2 U}{\partial y^2} \middle/ \frac{\partial \rho\langle uv \rangle}{\partial y} \right| \ll 1$$
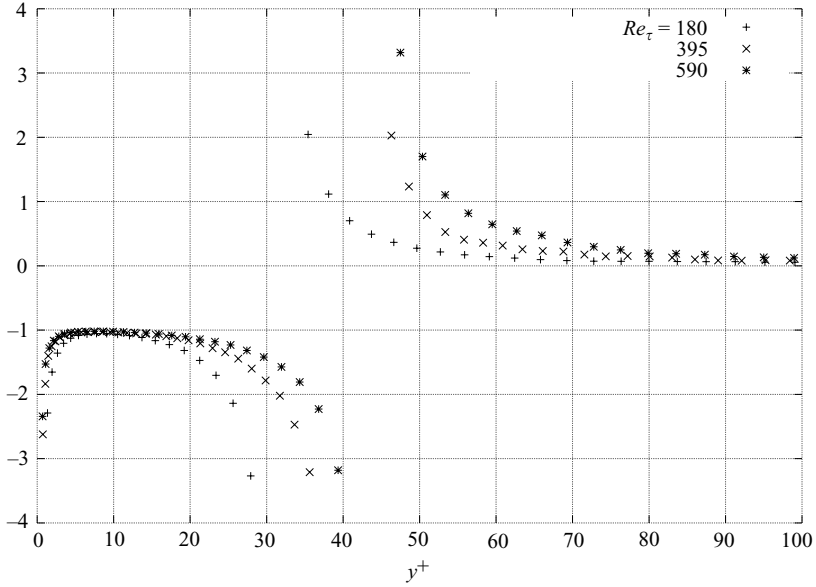
FIGURE 1. The ratio of the gradient of the viscous stress to the gradient of the Reynolds stress in fully developed channel flow, DNS data from Moser *et al.* (1999).

then the viscous force is small, and the pressure and Reynolds stress gradients are nominally in balance. If

$$\left| \mu \frac{\partial^2 U}{\partial y^2} \middle/ \frac{\partial \rho \langle uv \rangle}{\partial y} \right| \simeq 1,$$

their effects are in balance and the pressure gradient term is either of the same order or relatively smaller order. And, if

$$\left| \mu \frac{\partial^2 U}{\partial y^2} \middle/ \frac{\partial \rho \langle uv \rangle}{\partial y} \right| \gg 1$$

the Reynolds stress gradient is small and the pressure and viscous forces approximately balance.

Figure 1 shows the ratio of the gradient of the viscous stress to the gradient of the Reynolds stress for the fully developed channel flow, from the DNS of Moser, Kim & Mansour (1999). This figure shows a thin sublayer ($0 \leqslant y^+ \leqslant 3$) where pressure and viscous forces dominate the balance equation. Outside this thin layer is a region defined by a nearly perfect balance between the viscous and Reynolds stress gradients. The thickness of this stress-gradient balance layer shows a clear Reynolds-number dependence, extending well into the traditionally accepted logarithmic region of the mean velocity profile as Reynolds number increases. Near the location of maximum Reynolds stress, the viscous and pressure force are, once again, nearly in balance. Around the peak Reynolds stress location the gradient of the viscous stress is much larger than the gradient of the Reynolds stress. For greater distances from the wall, the Reynolds stress gradient changes sign and the viscous stress gradient becomes
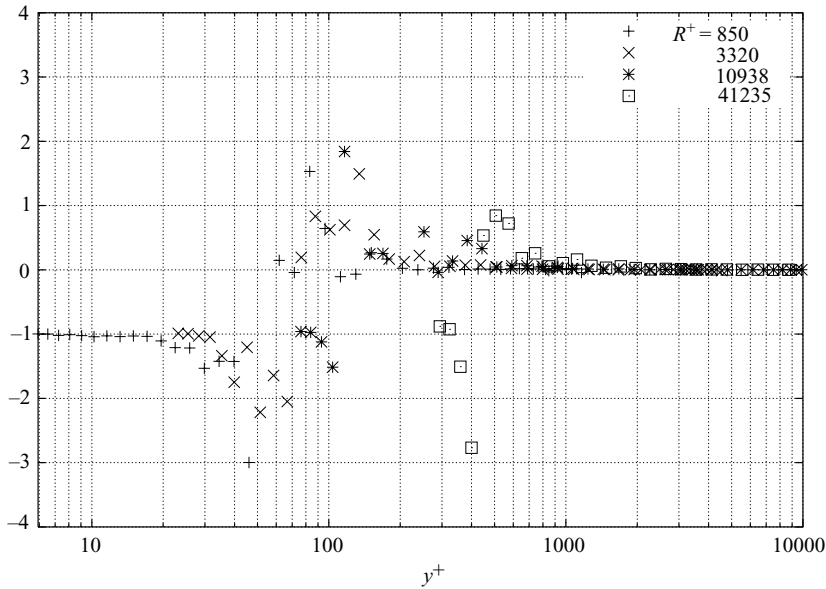
FIGURE 2. The ratio of the gradient of the viscous stress to the gradient of Reynolds stress in a turbulent pipe flow, as derived from the data of Zagarola & Smits (1997).

much smaller than either the Reynolds stress gradient or pressure gradient. In this region the Reynolds stress and pressure gradients are essentially in balance.†

The superpipe data of Zagarola & Smits (1997)‡ and the boundary layer data of Spalart (1988) and DeGraaff & Eaton (2000) exhibit similar behaviour. These data are plotted in figures 2 and 3 respectively. Both these sets of data show a Reynolds number dependence consistent with the DNS channel flow data in the inner region. For the superpipe data, the stress-gradient balance layer extends out to approximately $y^+ \cong 300$ at $R^+ \cong 41\,235$. Overall the turbulent boundary layer and superpipe data indicate that the width of the stress-gradient balance layer is Reynolds-number dependent and extends well into the traditionally accepted logarithmic layer. Existing superpipe data at higher Reynolds number cannot be reliably used to explore this issue further as the data point closest to the wall lies beyond the region of interest.

The behaviour of the ratio of the two stress-gradient terms as shown in figures 1–3, suggests a four-layer structure. The first region is an inner viscous/advection balance layer where the viscous force balances the pressure force (in channel flow), or in the case of the turbulent boundary layer the viscous force becomes smaller while balancing mean advection. (Note that all of the terms in equation (2.2) are zero at the wall in the zero-pressure-gradient boundary layer.) The second region is called the stress-gradient balance layer. In this layer the viscous and Reynolds stress gradients are of nearly equal magnitude but opposite sign. The third region is a meso viscous/advection balance layer where the viscous force balances the pressure force in channel flow or the mean advection in the turbulent boundary layer, while near the centre of this layer the Reynolds stress gradient passes through zero. The fourth region is

† A similar presentation of stress-gradient ratio data was earlier given by Cenedese, Romano & Antonia (1998), but only explored in the context of viscous sublayer structure.

‡ Note that the corrected superpipe data of McKeon *et al.* (2003) yields nearly identical results as Zagarola & Smits (1997) relevant to the present analyses.
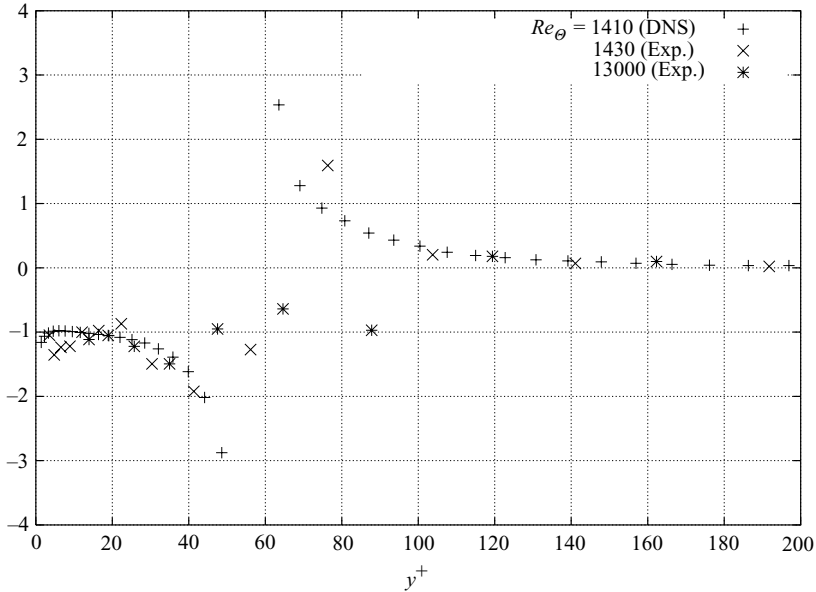
FIGURE 3. The ratio of the gradient of the viscous stress to the gradient of the Reynolds stress in turbulent boundary layers. DNS data are from Spalart (1988) and the experimental data are from DeGraaff & Eaton (2000).

an inertial/advection balance layer, where the Reynolds stress gradient balances the pressure force in channel flow or the mean advection in the turbulent boundary layer, while the viscous force is negligible. The sketch in figure 4 depicts the four layers as defined by the dynamics of the mean momentum balance at a fixed Reynolds number.

2.2. *Layer thicknesses*

Based on the DNS and laboratory data presented, the physical extent and the Reynolds-number dependence of each of the four layers identified above may be characterized. The inner viscous/advection sublayer extends from the wall to $y^+ \cong 3$, and, at most, exhibits only a very weak Reynolds number dependence. The stress-gradient balance layer extends from $y^+ \cong 3$ to $y^+ \cong 1.6 \times (\delta^+)^{1/2}$. For this characterization, the numerical constant of 1.6 is based on the criterion that the end of the stress-gradient balance layer is located where the ratio of the viscous to Reynolds stress gradients is less than -2. This definition is somewhat arbitrary in a fashion similar to the definition of δ_{99}. Further discussion regarding the definition of this layer is given in the theoretical considerations below. A meso viscous/advection balance layer extends from $y^+ \cong 1.6 \times (\delta^+)^{1/2}$ to $y^+ \cong 2.6 \times (\delta^+)^{1/2}$. (The numerical constant, 2.6, is determined by the criterion that the stress gradient ratio at the end of this layer decreases below 0.5.) Beyond the end of the meso viscous/advection balance layer, at $y^+ \cong 2.6 \times (\delta^+)^{1/2}$, is the inertial/advection balance layer, whose thickness is about $\delta^+ - 2.6 \times (\delta^+)^{1/2}$.

Except for the inner viscous/advection balance layer, the extent of these layers depends significantly on Reynolds number. The Reynolds-number dependence of the physical extent for each layer is shown in figure 5. Channel DNS data of Moser *et al.* (1999) and Superpipe data of Zagarola & Smits (1997) are used for the location of the end of the stress-gradient balance layer and the location of the end of the viscous/advection balance meso-layer. (The turbulent boundary layer data of DeGraaff &
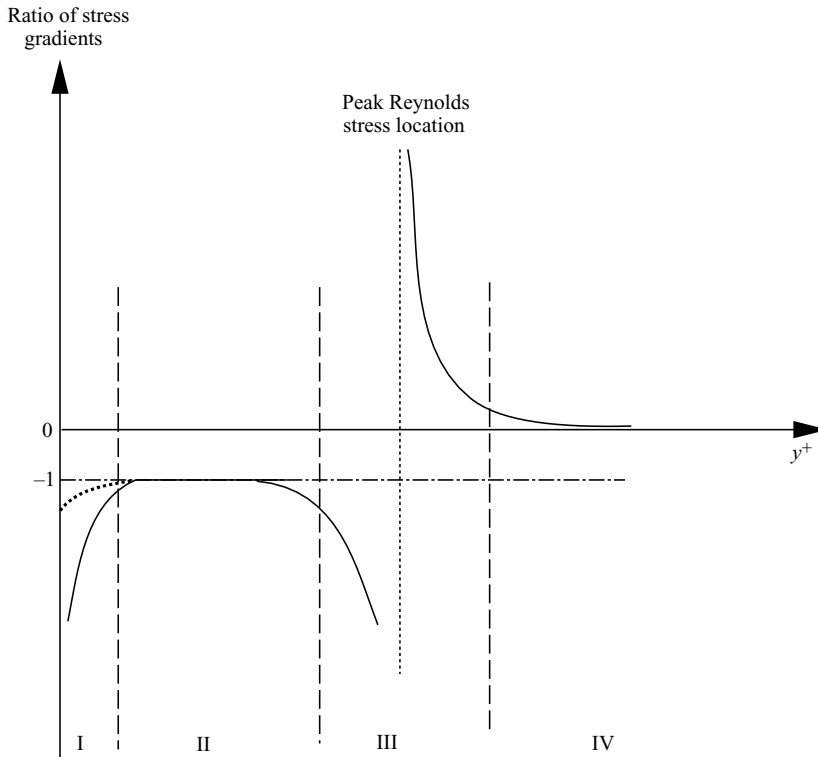
FIGURE 4. Sketch of the four layers of turbulent wall-bounded flows for one Reynolds number; layer I is the inner viscous/advection balance layer, layer II is the stress-gradient balance layer, layer III is the viscous/advection balance meso-layer and layer IV is the inertial/advection balance layer. Note layer I in the zero-pressure-gradient turbulent boundary layer is different from that of channel and pipe flow in that all of the terms in equation (2.2) are zero at the wall.

Eaton (2000) has been tried, but the second derivative of the mean profile and the derivative of Reynolds stress are noisy.) As is evident, all of the Reynolds-number dependences can be tied to the growth rate of the stress-gradient balance layer thickness. For this reason, the thickness of this layer is identified as an important intermediate length since, like all similarity variables, it arises solely from the internal dynamics of the problem. Along with the outer and inner scales, δ and ν/u_τ respectively, the analyses below show that this meso-scale, $\sqrt{\nu\delta/u_\tau}$, is fundamental to the description of the mean flow.

As indicated in figure 5, the thickness of the inertial/advection balance layer is $\delta^+ - 2.6 \times (\delta^+)^{1/2}$, the ratio of this layer thickness to the total layer thickness, δ^+, is then $1 - 2.6 \times (\delta^+)^{-1/2}$. This is illustrated in figure 6, which shows that the inertial/advection layer is an increasingly larger fraction of the entire boundary layer with increasing Reynolds number. For example, this layer constitutes about 95.2%, 99.1% and 99.7% of the boundary layer thickness at $\delta^+ \cong 3000$, $\delta^+ \cong 10^5$ and $\delta^+ \cong 10^6$ respectively. Figure 6 is a linear–linear plot. These axes were chosen to best illustrate the behaviour of the inertial/advection layer at low to moderate Reynolds number. As the Reynolds number decreases, the ratio of the thickness of this layer to δ decreases rapidly. For example, the inertial/advection layer is about 74.0%, 81.6%
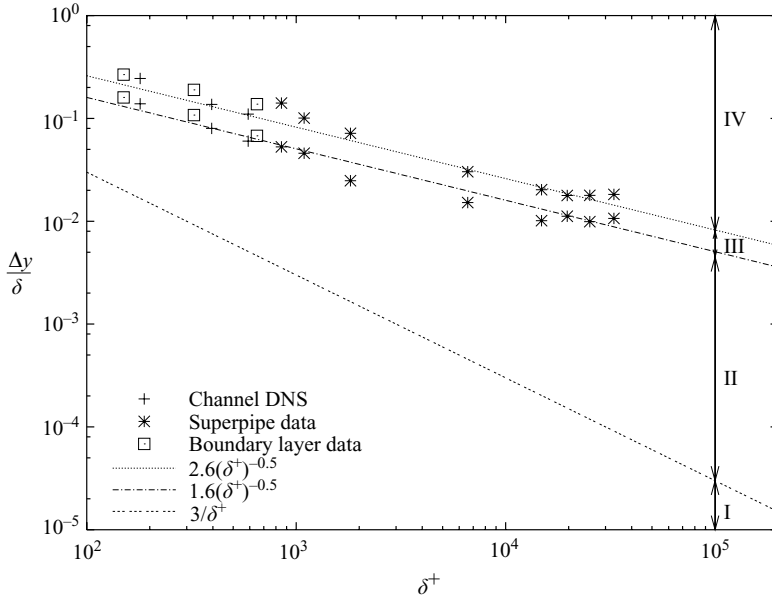
FIGURE 5. Reynolds-number dependence of the outer-normalized physical extent of the four layers in canonical wall flows. The four layers are numbered according to the sketch of figure 4. Channel data are from Moser *et al.* (1999), pipe data are from Zagarola & Smits (1997) and turbulent boundary layer data are from Spalart (1988).
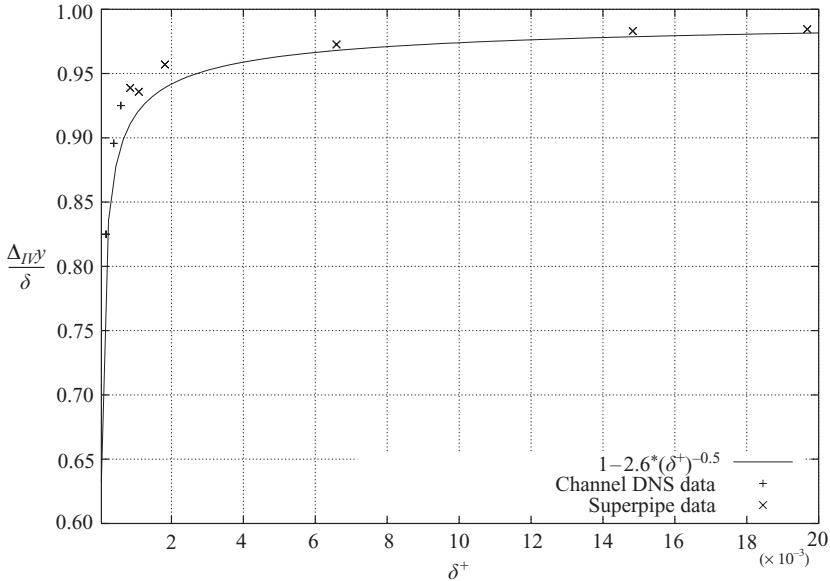

FIGURE 6. Reynolds-number dependence of the ratio of the inertial/advection layer thickness to the boundary layer thickness. Note the Reynolds number on the abscissa is δ^+. For reference, Re_θ for the zero-pressure-gradient turbulent boundary layer flow is typically about $3 \sim 4$ times that of the corresponding δ^+.
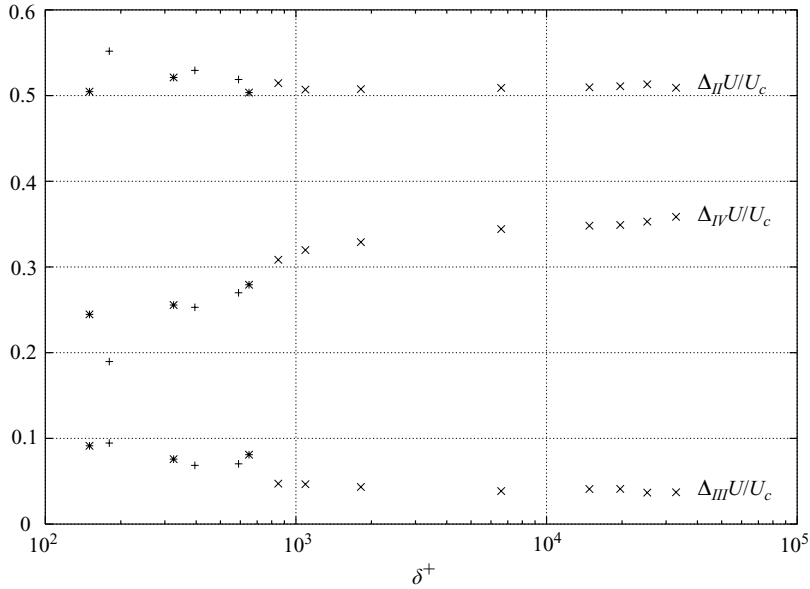
FIGURE 7. Outer normalized velocity increments across the layers as depicted in figure 4: $+$, channel data, of Moser *et al.* (1999); $\times$, superpipe data of Zagarola & Smits (1997); $*$, turbulent boundary layer data of Spalart (1988). $\Delta_{II}U$ is the velocity increment across the stress-gradient balance layer, $\Delta_{III}U$ is the velocity increment across the meso viscous/advection balance layer and $\Delta_{IV}U$ is the velocity increment across the inertial/advection balance layer.

and 88.3% of δ at $\delta^+ \cong 100$, $\delta^+ \cong 200$, $\delta^+ \cong 500$ respectively). These rapid changes at low Reynolds number are likely to correspond with other significant changes in boundary layer properties. In this regard, there is an increasing body of evidence (e.g. Klewicki 1989; DeGraaff & Eaton 2000) that the scaling properties of turbulence quantities largely break down at sufficiently low but still fully turbulent Reynolds numbers. The rapid change of scale effects of the inertial/advection balance layer may provide the underlying reason for these observations.

2.3. *Velocity increments*

Owing to the fact that it is zero outside the boundary layer and non-zero inside the boundary layer, vorticity, and its wall-normal distribution, are particularly relevant measures of turbulent wall-flow structure. For a two-dimensional flow in the (x, y)-plane, the circulation, Γ, is a useful integral measure of the total mean z-component vorticity present. In the case of the boundary layer (or half-channel), it is easy to show that, per unit length, the circulation of the entire layer has a magnitude equalling the total velocity increment across the layer, i.e. $|\Gamma_{total}| = U_\infty$.

Given this, and for the purposes of better understanding the distribution of vorticity across the four balance layers (as well as the Reynolds number dependence of these distributions), the velocity increment across each balance layer was determined as a function of Reynolds number. These results are shown in figure 7. Under outer normalization, the velocity increment across the stress-gradient balance layer is essentially constant, equalling about 50% of the total velocity increment. The velocity increment across the inertial/advection balance layer increases rapidly at low Reynolds number and then levels off to a slower rate of increase over the Reynolds number range shown. The initial rapid increase reflects the changes in the mean profile wake structure at low

R_θ. In contrast, the velocity increments across the inner and meso viscous/advection layers become a decreasingly small fraction of U_∞ with increasing Reynolds number. If the scalings discussed here for layers I, II, and III continue to hold for high Reynolds number, the velocity increment across layer IV will asymptotically approach 50% of U_∞. On the other hand, inner normalization (not shown here) of the velocity increments across the inner and meso viscous/advection layers are essentially invariant with Reynolds number, equal to about $3u_\tau$ and $1u_\tau$ respectively. As expected, the inner normalized velocity increments across the stress-gradient balance layer and inertial/advection layer increase like U_∞^+. It is intriguing to note that while the meso viscous/inertial layer grows like $\sqrt{\delta^+}$ with increasing Reynolds number, its position in the layer is such that the inner normalized velocity increment across it remains essentially constant. Similarly, it is worth noting that the circulation of the stress-gradient balance layer is apparently independent of Reynolds number, $0.5|\Gamma_{total}|$.

2.4. *Data summary*

The above experimental results have a number of implications. Perhaps most important is that viscous effects are dynamically significant from the wall out to a (Reynolds-number-dependent) position beyond the peak in the Reynolds stress. At large but technologically relevant Reynolds numbers this position could be thousands of viscous units from the surface. Thus, the nearly universally held notion, e.g. Tennekes & Lumley (1972), Gad-el-Hak & Bandyopadhyay (1994), George & Castillo (1997), Pope (2000), that viscous effects are, in the mean, dynamically negligible outside the buffer layer ($y^+ \simeq 30$) is not supported by the relevant stress-gradient data. The relevance of such viscous effects was an emphasis of the work of Sahay (1997). Coupled to this misconception is the commonly employed approximation that outside the buffer layer equation (2.1) is well represented by a balance between the pressure and Reynolds stress gradients, as is the misconception that the traditionally defined logarithmic layer (say $y^+ \geqslant 30$ to $y/\delta \leqslant 0.15$) is a zone of nominally zero Reynolds stress gradient, e.g. Wosnik *et al.* (2000). That is, the traditional logarithmic layer encompasses portions of layers II and IV and all of layer III. This provides a reason to rationally question the efficacy of the representation of the traditional logarithmic layer as the overlap region between an inner and outer layer, Millikan (1939). In fact, the empirical observations suggest the existence of a third, intermediate, dynamical length scale. These and a number of other related observations are given theoretical foundation by the analyses that follow.

3. Scale analysis of turbulent channel flow

Concepts of multiscale analysis are applied here to the problem of statistically stationary, fully developed turbulent flow in a two-dimensional channel. The reasoning employed corroborates and adds to the understanding of the four-layer structure revealed by the above data presentation. It is shown that the analysis is most properly done using three length scales, each appropriate to its own region.† The orders of magnitude of the widths of the scaling regions are given, as well as the governing equations in each of the regions and some qualitative features of the flow in each. The question of the merging of adjacent scaling domains is discussed. For completeness, some scaling results that are already well-known are included.

---

† Work in progress (Fife *et al.* 2004) shows that there is a hierarchy of length scales which serve to smoothly connect the inner, meso and outer scales. These results are forthcoming.

The discussion is systematic, relying only on the averaged momentum equation and as few other assumptions as possible. For example, one important assumption is that U^+ monotonically increases, and its gradient monotonically decreases from the wall to the centreline:

$$\frac{\mathrm{d}U^+}{\mathrm{d}y^+} > 0, \quad \frac{\mathrm{d}U^+}{\mathrm{d}y^+} \text{ decreases from 1 (at the wall) to 0 at the centreline and}$$

$$U_c^+ \to \infty \text{ as } \delta^+ \to \infty, \quad (3.1)$$

where U_c^+ is the mean velocity at the centreline.

At this juncture it is worth putting this paper's approach in perspective with what will be called the *classical* approach. The classical approach purports to derive salient properties of the velocity and Reynolds stress profiles by means of the inner and outer scales alone. Based on the suggestion of Izakson (1937) and Millikan (1939) and exemplified by many later writers such as Afzal (1976, 1982, 1984a) and Panton (1990), whose work is possibly most completely expounded in Panton (2003) and Buschmann & Gad-el-Hak (2003), it is assumed, in the classical scenario, that an overlap region of the flow exists, in which the traditional outer and inner forms of the mean velocity profile are simultaneously valid. Incidentally, Gill (1968) rightly showed that at the very least, additional assumptions about the magnitude of the errors in these approximations are needed (such assumptions, as well as assumptions about the location of the overlap zone, would be difficult to validate in an *a priori* manner). If these estimates are valid, then matching derivatives in the overlap zone produces an equation whose solution for the velocity profile is either (*a*) $U^+ = $ constant or (*b*) U^+ grows logarithmically. Conclusion (*a*) is unacceptable, since it is known from (3.1) that U^+ is a strictly increasing function of distance from the wall.

In the present paper, the meso-layer scaling is shown analytically to have the same legitimacy as the inner and outer scalings, in the sense that the meso-layer is shown theoretically to necessarily exist, by reasoning as valid as any theoretical basis for the traditional scalings. Given this, the classical, two-layer, description would appear to constitute an incomplete framework for the problem. In addition, concerns arise about the derivation itself. A derivation, such as the classical one just described, should proceed in a logical manner from assumptions that are both credible and removed from the conclusion that is being derived. In this sense, it seems rational to question whether it is reasonable to assume the existence of an overlap zone in which the profile is not constant.

The motivation for this concern arises from two observations:

(i) Although the existence of overlap zones associated with two-scale problems in other fields and with mathematical examples is prevalent and well-known, the profile is generally constant in the overlap zone.

(ii) There are any number of functions with two scales which reduce to the given outer/inner forms in the outer/inner scaling domains, but do not have overlap zones nor logarithm profiles. In view of this, one must ask whether there is some natural physical reason why one should consider only profiles with overlap zones. This would be an interesting subject of further investigation.

Therefore, while recognizing that many of the present results could be interpreted or corroborated on the basis of the logarithmic profile emerging from classical Millikan-type arguments, assumed valid in some appropriate region, it is felt that an alternative approach, which would serve as a comparison and contrast with the classical one, is highly desirable. Regarding this point, it is also worth noting the lucid arguments of

Sahay (1997) that advocate the benefits of a 'first principles' approach not reliant on the overlapping layer hypothesis. Consistent with this, the derivations presented in this paper are totally independent of the classical train of thought.

3.1. *Momentum balance properties in the four layers*

In terms of the traditional inner variables y^+, U^+, and $T^+ \equiv -\langle uv \rangle^+$, the conservation equation for streamwise momentum is

$$\frac{\mathrm{d}^2 U^+}{\mathrm{d}y^{+2}} + \frac{\mathrm{d}T^+}{\mathrm{d}y^+} + \epsilon^2 = 0, \tag{3.2}$$

where the small parameter $\epsilon = 1/\sqrt{\delta^+}$, $\delta^+ = u_\tau \delta/\nu$ is used so that $\epsilon \to 0$ as $Re \to \infty$. Associated with (3.2) are the boundary conditions

$$U^+ = T^+ = 0 \text{ and } \frac{\mathrm{d}U^+}{\mathrm{d}y^+} = 1 \text{ at } y^+ = 0. \tag{3.3}$$

The traditional outer variables are η, U^+, T^+, where $\eta = \epsilon^2 y^+ = y/\delta$. (The centreline is at $y = \delta$.) Alternatively, the variable U^+ in this list is often replaced by the defect velocity $U_c^+ - U^+$. Equation (3.2) becomes

$$\frac{\mathrm{d}T^+}{\mathrm{d}\eta} + 1 + \epsilon^2 \frac{\mathrm{d}^2 U^+}{\mathrm{d}\eta^2} = 0, \tag{3.4}$$

with boundary conditions

$$T^+ = \frac{\mathrm{d}U^+}{\mathrm{d}\eta} = 0 \text{ at } \eta = 1. \tag{3.5}$$

It will be shown from scaling arguments alone that an intermediate scaling with its layer (III) exists as well, thus corroborating the empirical finding described in the previous section. All this will result in three different forms for the momentum equation: (3.2), (3.4), and later (3.19).

Equation (3.2), while correct in all cases, is the most appropriate of the three forms of the momentum equation to use in regions where the two derivatives indicated there are $\leqslant O(1)$, and at least one is not small ($o(1)$). (Here and below, all order of magnitude relations are understood to hold as $\epsilon \to 0$, and the order symbols, O and o, take their established definitions, e.g. Kevorkian & Cole (1981), with the exception that a relation $a = O(1)$, say, means that both a and $1/a$ are bounded as $\epsilon \to 0$.) This is the case near the wall in layers I and II. When at least one of the first two terms in (3.2) is not small, i.e. $O(\epsilon^2)$, the third term in equation (3.2) may be neglected, leaving

$$\frac{\mathrm{d}^2 U^+}{\mathrm{d}y^{+2}} + \frac{\mathrm{d}T^+}{\mathrm{d}y^+} = 0. \tag{3.6}$$

Integrating with use of (3.3) yields

$$\frac{\mathrm{d}U^+}{\mathrm{d}y^+} + T^+ - 1 = 0. \tag{3.7}$$

Similarly in the region where the derivatives appearing in (3.4) are $\leqslant O(1)$ and $\mathrm{d}T^+/\mathrm{d}\eta$ is not small, such as near the midline $\eta = 1$, the $O(\epsilon^2)$ term in (3.4) may be neglected, leaving

$$\frac{\mathrm{d}T^+}{\mathrm{d}\eta} + 1 = 0, \tag{3.8}$$

and integrated to obtain

$$T^+(\eta) = 1 - \eta. \tag{3.9}$$

The solution $T^+(\eta)$ given by (3.9) approaches the limit 1 as $\eta \to 0$, instead of 0 as it should do according to (3.3). Thus there is a region near the wall where the stated condition on which the validity of (3.8) depends breaks down. In this wall layer, T^+ drops abruptly to 0 as $\eta \to 0$; the T^+ derivative in (3.4) then gets very large. From this one can surmise the known fact that T^+ attains a maximal value, say $T_m^+(\epsilon)$, near the wall. (The extra assumption that $\mathrm{d}^2U^+/\mathrm{d}y^{+2}$, which is negative, increases towards 0, when applied to (3.2), would entail T^+ having only a single maximum.) The value of y^+ at which $T^+ = T_m^+$ is designated by $y_m^+(\epsilon)$, and the corresponding value of η by $\eta_m(\epsilon) = \epsilon^2 y_m^+(\epsilon)$.

   Although $T_m^+(\epsilon)$ and $y_m^+(\epsilon)$ are unknown at this point, certain general conclusions can be drawn about them. One is that, $T_m^+ < 1$ since the outer solution (3.9) satisfies that inequality. And since mathematical boundary layers get thinner as the perturbation parameter approaches zero, the position $\eta_m(\epsilon) \to 0$ as $\epsilon \to 0$. Finally, another way of saying this is that the domain where the outer solution is valid expands towards the wall as $\epsilon \to 0$, i.e. (3.9) is valid for values of η in intervals $\eta_0(\epsilon) \leqslant \eta \leqslant 1$, where $\lim_{\epsilon \to 0} \eta_0(\epsilon) = 0$. Thus,

$$\lim_{\epsilon \to 0} T_m^+(\epsilon) = 1. \tag{3.10}$$

3.1.1. *Layers I and II*

   These are where the inner variables are appropriate. Layer I is the viscous sublayer and layer II is where the viscous and Reynolds stress gradients are balanced. The viscous sublayer is where y^+ is so small (recall $T^+(0) = 0$) that $T^+(y^+) \cong 0$ is negligible. Then from (3.7) and (3.3),

$$U^+ \approx y^+. \tag{3.11}$$

   Integrating (3.2) gives

$$\frac{\mathrm{d}U^+}{\mathrm{d}y^+} = 1 - T^+ - \epsilon^2 y^+. \tag{3.12}$$

The small ϵ^2 term is included here, because this equation will soon be used a little outside the formal range of validity of the approximate version (3.6), namely where layer II merges with layer III. As previously mentioned, when the last term in (3.12) is small (such as when $y^+ = O(1)$), it may be neglected. In any case, (3.12) shows how to find U^+ if the function $T^+(y^+)$ were known. It is, of course, unknown. But it was brought out before that $T^+(0) = 0$ and $T^+(y^+)$ increases to its maximum value $T_m^+(\epsilon)$ at $y^+ = y_m^+(\epsilon)$. By (3.10) the maximum falls just short of 1. It follows then from (3.12) that the gradient $\mathrm{d}U^+/\mathrm{d}y^+$ starts at 1 at $y^+ = 0$, and decreases to a small value at $y_m^+(\epsilon)$, provided that $\epsilon^2 y_m^+(\epsilon) \ll 1$. This will be verified later. A function quantifying the deviation of T_m^+ from its upper limit of 1 is

$$\sigma(\epsilon) = 1 - T_m^+(\epsilon). \tag{3.13}$$

Although positive, it approaches 0 with ϵ. Further details regarding the order of magnitude of σ will be given later.

3.1.2. *Layer III*

   This is the meso-layer containing $T_m(\epsilon)$; similar concepts have been described using different tools by others, e.g. Long & Chen (1981), Afzal (1982, 1984a), Sahay (1997), Sreenivasan & Sahay (1997), George & Castillo (1997). For example, Sahay

combined empirical data and theoretical reasoning to study the scaling properties of the Reynolds stress profile, and hence velocity profile, near the location of its peak (Sahay 1997). He presented strong evidence that a meso-layer exists, and noted that data indicate its location and characteristic lengths to be in agreement with what is found by purely theoretical methods in the present paper. For present purposes this layer may roughly be defined as where the approximations made above – replacing (3.2) by (3.6) and dropping the last term in (3.12) are no longer valid, because the term dropped is no longer smaller (in order of magnitude) than both of the other two individual terms in those equations. The transition out of layer II may be described in the following way. For moderate values of y^+ outside layer I, the first two terms in (3.2) are each $O(1)$, and except for an $O(\epsilon^2)$ difference, they cancel each other. As y^+ increases, each of the first two terms decreases in magnitude; the second term does so because T^+ approaches its maximum, and therefore (3.2) itself forces the magnitude of the first term also to decrease. Eventually, $\mathrm{d}T^+/\mathrm{d}y^+ = O(\epsilon^2)$, and by (3.2) $|\mathrm{d}^2U^+/(\mathrm{d}y^+)^2| \leqslant O(\epsilon^2)$. To be more specific, albeit still arbitrary, let y_1^+ be the value of y^+ at which $\mathrm{d}^2U^+/(\mathrm{d}y^+)^2 = -2\epsilon^2$. A tentative definition for the transition point between layers II and III is this location $y_1^+(\epsilon)$, although in reality the boundary is not well-defined. This choice corresponds to the definition given in §2.2, i.e. the point where $\mathrm{d}^2U^+/(\mathrm{d}y^+)^2/\mathrm{d}T^+\mathrm{d}y^+ = -2$.

The same may be done with (3.12). Again, for moderate values of y^+, it represents an approximate balance between the quantities $\mathrm{d}U^+/\mathrm{d}y^+$ and $1-T^+$, with error $\epsilon^2 y^+$. As y^+ increases, those two terms decrease and $\epsilon^2 y^+$ increases, until both $\mathrm{d}U^+/\mathrm{d}y^+$ and $1-T^+$ are $\leqslant O(\epsilon^2 y^+)$. Again to be specific, let $y_2^+(\epsilon)$ be the location where $\mathrm{d}U^+/\mathrm{d}y^+(y_2^+) = 2\epsilon^2 y_2^+$; this is once more an arbitrary criterion. At that point, $1-T^+ = 3\epsilon^2 y_2^+$ by (3.12).†

Two possible definitions for the transition point between layers II and III, found by similar constructions, are now given by $y_1^+(\epsilon)$ and $y_2^+(\epsilon)$. It is reasonable to expect that at least in order of magnitude, they are the same. This can be verified to be true in the typical case that $\mathrm{d}U^+/\mathrm{d}y^+$ asymptotically decays for large y^+ according to a power law:

$$\frac{\mathrm{d}U^+}{\mathrm{d}y^+} \approx C(y^+)^{-m} \quad \text{for some } m > 0, \ C > 0, \tag{3.14}$$

with the corresponding relation holding after differentiation: $\mathrm{d}^2U^+/(\mathrm{d}y^+)^2 \approx -mC(y^+)^{-m-1}$. For in this case, y_1^+ and y_2^+ are both $O(\epsilon^{-2/(m+1)})$. (Actually, the decay assumption here can be relaxed to hold only up to $y^+ = y_1^+(\epsilon)$, because a different scaling for the function U^+ will be used for greater y^+.) It is also allowed that C depends on ϵ, as $C = C'\epsilon^\alpha$, where $\alpha < 2$. In addition, the experimentally and computationally determined values of the two numbers shown in table 1 give strong support to the expectation that $y_1^+ \approx y_2^+$ (they both are seen to be $O(1/\epsilon)$). The transition point is therefore specifically defined to be $y_1^+(\epsilon)$.

The location $y^+ = y_1^+$ was designated as the lower edge of layer III, and in an analogous fashion the location $y^+ = y_3^+$ where $\mathrm{d}^2U^+/(\mathrm{d}y^+)^2 = -\frac{1}{3}\epsilon^2$ is defined to be the upper edge, because that corresponds to where $\mathrm{d}^2U^+/(\mathrm{d}y^+)^2/\mathrm{d}T^+/\mathrm{d}y^+ = \frac{1}{2}$, as was done in the experimental data analysis in §2.2.

At the transition point $y_1(\epsilon)$, each of the first two terms in (3.2) is $O(\epsilon^2)$, although their formal appearance in that equation does not indicate this fact. This is the

† The authors have discovered a more straightforward theoretical method to find the location of this and other layers, using a hierarchy of scales (Fife *et al.* 2004).

Re_τ	y_1^+	y_2^+	$y_1^+/(1/\epsilon)$	$y_2^+/(1/\epsilon)$
180	25.1	20.2	1.88	1.51
395	31.7	26.2	1.60	1.32
590	36.7	30.5	1.51	1.26
850	44.3	35.8	1.52	1.23
2344.7	54	48.4	1.12	0.999
8486.3	79.6	80.5	0.864	0.873

TABLE 1. Locations of y_1 and y_2. Data are from Moser *et al.* (1999) and Zagarola & Smits (1998).

beginning of layer III, and a rescaling will now be sought to better reflect the true orders of magnitude of the terms in (3.2). In fact, a scaling is possible that renders all three terms formally the same order of magnitude. In the process, additional information regarding $\sigma(\epsilon)$ and $T_m^+(\epsilon)$ will be revealed. The existence and scaling of a third layer was possibly first found by Afzal (1982, 1984*a*).

The rescaled y^+ and T^+ variables will be called $\hat{y}$ and $\hat{T}$. Rescaling is most easily accomplished for the differentials dy^+ and dT^+; explicit expressions for the new variables, in terms of the old ones, will be derived later. With factors α and β to be determined (they will depend on ϵ), rescaling begins by setting

$$dy^+ = \alpha d\hat{y}, \quad dT^+ = \beta d\hat{T}. \tag{3.15}$$

This transforms the terms in (3.2) as follows:

$$\frac{d^2U^+}{(dy^+)^2} = \frac{1}{\alpha^2}\frac{d^2U^+}{d\hat{y}^2}, \quad \frac{dT^+}{dy^+} = \frac{\beta}{\alpha}\frac{d\hat{T}}{d\hat{y}}. \tag{3.16}$$

The idea now is to assume that the derivatives on the right of (3.16), namely $d^2U^+/d\hat{y}^2$ and $d\hat{T}/d\hat{y}$, are $O(1)$ quantities. By the requirement established above, the orders of magnitude of both terms on the right, namely $1/\alpha^2$ and β/α, must match (in order of magnitude) the third term in (3.2), namely ϵ^2: $\alpha^{-2} = \beta/\alpha = \epsilon^2$. This is only possible if $\beta = \epsilon, \alpha = \epsilon^{-1}$. Thus from (3.15)

$$d\hat{y} = \epsilon dy^+, \quad dT^+ = \epsilon d\hat{T}. \tag{3.17}$$

Integrating (3.17) gives two integration constants, which are chosen to be y_m^+ and T_m^+; they will be the values of y^+ and T^+ where $\hat{y} = 0$ and $\hat{T} = 0$. The result is

$$y^+ = y_m^+ + \frac{1}{\epsilon}\hat{y}, \quad T^+ = T_m^+ + \epsilon\hat{T}. \tag{3.18}$$

Thus the scaling to be employed in layer III is now completely defined, along with its lower and upper edges $y_1^+(\epsilon)$ and $y_3^+(\epsilon)$. With the transformation (3.18), (3.2) becomes

$$\frac{d^2U^+}{d\hat{y}^2} + \frac{d\hat{T}}{d\hat{y}} + 1 = 0. \tag{3.19}$$

Now consider the balancing property of (3.12). As in the case of (3.2), it suffices at the transition point, $y^+ = y_2^+(\epsilon)$, to require that the three terms dU^+/dy^+, $(1-T^+)$, $\epsilon^2 y_2^+$ in (3.12) have the same formal order of magnitude. Those orders can be calculated as follows. Since, by definition, $\hat{y}$ and $dU^+/d\hat{y}$ are both $O(1)$ in layer III, it follows that $|dU^+/dy^+| = \epsilon|dU^+/d\hat{y}| = O(\epsilon)$ (This is supported by the data as shown in table 2). As for the second term in (3.12), write it as $1-T^+ = (1-T_m^+) + (T_m^+ - T^+) = \sigma - \epsilon\hat{T}$,

Re_τ	$dU^+/dy^+\|_{y^+=2/\epsilon}$	$(dU^+/dy^+\|_{y^+=2/\epsilon})/\epsilon$
180	0.135	1.802
395	0.066	1.307
590	0.050	1.211
850	0.035	1.029
2344.7	0.0191	0.927
8486.3	0.0126	1.156

TABLE 2. Experimentally determined dU^+/dy^+ values at $y^+ = 2/\epsilon$ (inside the meso-layer, around the peak Reynolds stress location). Data are from Moser *et al.* (1999) and Zagarola & Smits (1998).

Re_τ	σ	ϵ	σ/ϵ
180	0.275	0.075	3.67
395	0.162	0.0505	3.21
590	0.135	0.0413	3.27
850	0.10	0.034	2.94
2344.7	0.061	0.0206	2.96
8486.3	0.0328	0.0109	3.01

TABLE 3. Experimentally determined σ values. Data are from Moser *et al.* (1999) and Zagarola & Smits (1998).

so that since $\hat{T} \leqslant O(1)$, $1 - T^+ = O(\max[\sigma, \epsilon])$. And of course the last term is $\epsilon^2 y_2^+$. Equating the three orders of magnitude yields

$$\max[\sigma, \epsilon] = O(\epsilon), \quad \epsilon^2 y_2^+ = O(\epsilon). \tag{3.20}$$

This implies that

$$\sigma \leqslant O(\epsilon) \quad \text{and} \quad y_2^+ = O(\epsilon^{-1}). \tag{3.21}$$

Setting $y^+ = y_m^+$ in (3.12) and using (3.1) gives

$$\sigma = 1 - T_m^+ = \frac{dU^+}{dy^+}(y_m^+) + \epsilon^2 y_m^+(\epsilon) \geqslant O(\epsilon). \tag{3.22}$$

(An argument like this was also supplied in Sreenivasan & Sahay (1997).) Combining (3.22) with (3.21) gives

$$\sigma = O(\epsilon). \tag{3.23}$$

The data of table 3 and figure 8 support these theoretical predictions.

Throughout layer III, U^+, $\hat{T}$ and their derivatives are, to lowest order in ϵ, regular functions of the rescaled variable $\hat{y}$. To justify this assertion, consider that the momentum equation written in terms of $\hat{y}$, (3.19), has no ϵ-dependence, and on each end of layer III, i.e. at $y^+ = y_1^+$ and y_3^+, each term of that equation is $O(1)$. In fact, $d^2U^+/d\hat{y}^2 = -2$ at the lower end, and $= -\frac{1}{3}$ at the upper end. We take this to be conclusive evidence that those derivatives, and their derivatives in turn, remain $O(1)$ in III. The width of layer III can now be found. It will be gauged by $\Delta\hat{y} = \hat{y}_3 - \hat{y}_1$ (corresponding to $y_3^+ - y_1^+$). The corresponding increment in $d^2U^+/d\hat{y}^2$ is

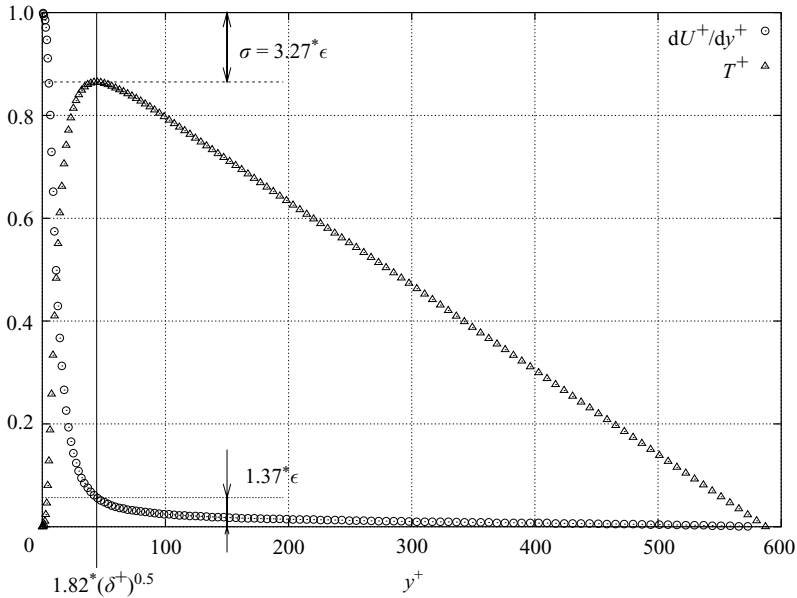$$\Delta\frac{d^2U^+}{d\hat{y}^2} = -\frac{1}{3} - (-2) = \frac{5}{3}.$$

FIGURE 8. Properties of viscous shear stress and Reynolds shear stress compared to the present theory. In the meso-layer $\sigma = O(\epsilon)$ and $dU^+/dy^+ = O(\epsilon)$. Data are from Moser *et al.* (1999) $Re_\tau = 590$.
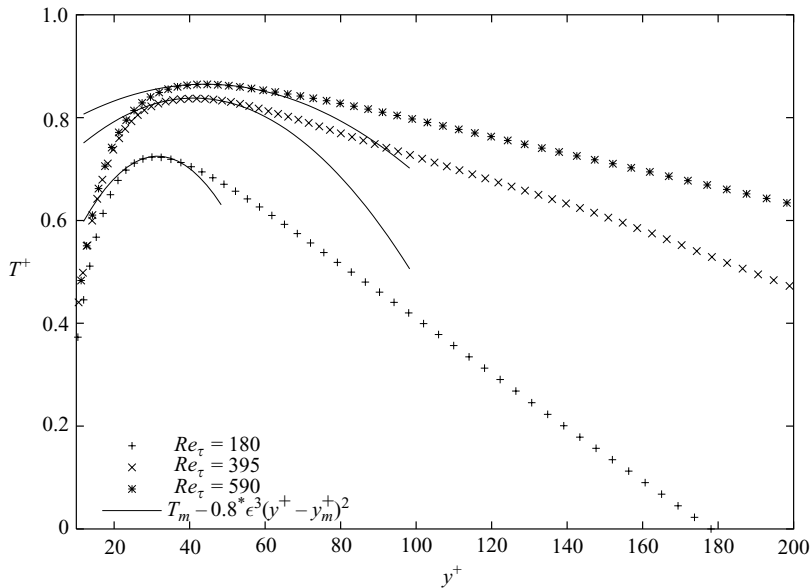

FIGURE 9. Reynolds stress around the peak, showing $d^2T^+/dy^{+2} = O(\epsilon^3)$. Data are from Moser *et al.* (1999).

but for some value $\hat{y}^*$ in layer III, the mean value theorem says that the left-hand side $= d^3U^+/d\hat{y}^3(\hat{y}^*)\Delta\hat{y}$, so that $\Delta\hat{y} = k$ where $k = \frac{5}{3}(d^3U^+/d\hat{y}^3)^{-1}$. By differentiating (3.19) and using the data from figure 9, which shows that $|d^2\hat{T}d\hat{y}^2| = |d^3U^+/d\hat{y}^3|$ is $O(1)$, one finds

$$\Delta\hat{y} = O(1). \tag{3.24}$$

Therefore the width of layer III $= O(1)$ in the variable $\hat{y}$, i.e. $O(1/\epsilon)$ in y^+.

In summary, layer III is characterized in part by

$$|\hat{y}| = O(1), \ y^+ = O(1/\epsilon), \ \frac{\mathrm{d}U^+}{\mathrm{d}y^+} = O(\epsilon), \ \frac{\mathrm{d}U^+}{\mathrm{d}\hat{y}} = O(1);$$

$$\text{the higher derivatives of } \frac{\mathrm{d}U^+}{\mathrm{d}\hat{y}} \text{ and } \hat{T} \text{ are } O(1). \quad (3.25)$$

3.1.3. *Qualitative implications of the scaling in layer III*

Since by definition $y_1^+(\epsilon)$ is the transition point between layers II and III, and layer I has width (in y^+) $O(1)$, the second part of (3.21) says that the width of layer II is $O(\epsilon^{-1})$. This is the first important consequence of the scaling in layer III. In connection with this it is relevant to note that this result of the analysis is in complete accord with the experimental data. The second important property of layer III comes from the fact (see (3.25)) that $\mathrm{d}U^+/\mathrm{d}\hat{y} = O(1)$ in layer III, i.e. where $|\hat{y}| \leqslant O(1)$. Integrating across the layer, it is found that the velocity increment $\Delta_{III}U^+$ across the layer is an $O(1)$ quantity. The significance is that it is (approximately) independent of δ^+, which is also in explicit agreement with the experimental observations.

A third qualitative effect in layer III concerns the pronounced flattening in the $T(y^+)$ profile near $T^+ = T_m^+$, as seen for example in Sreenivasan & Sahay (1997). This can be explained by measuring the curvature by the second derivative of the function T^+. With the meso-scaling which has been seen to be appropriate in layer III, it follows that $\hat{T}$ is a regular function of $\hat{y}$, so that in particular, it is expected that $\mathrm{d}^2\hat{T}/(\mathrm{d}\hat{y})^2 = O(1)$. In view of (3.17), this means that $\mathrm{d}^2T^+/(\mathrm{d}y^+)^2 = O(\epsilon^3)$ and $\mathrm{d}^2T^+/\mathrm{d}\hat{y}^2 = O(\epsilon)$. This is smaller (flatter) than one might anticipate. On the other hand, the second derivative with respect to the outer variable η at $\eta = \eta_m$ is, as expected, large, so that the profile from the outer perspective is still sharply peaked. The flattening effect of T^+ near T_m^+ is explicitly shown to follow the predicted behaviour in figure 9.

It is appropriate to reiterate an assumption which was made here in connection with the characterization of layer III. A scaling was found and an interval $[y_1^+, y_3^+]$ was found for which (i) an ϵ-independent differential equation (3.19) holds, expressing a balance between at least two kinds of scaled forces, and (ii) the derivatives in (3.19) are verified to be $O(1)$ on each end of the interval (this latter condition is usually disregarded by other authors). It was then inferred that the physical quantities U^+ and $\hat{T}$ do in fact satisfy (3.19) to lowest order, and that they and their higher derivatives are $O(1)$ within the interval. More generally, it is reasonable to relax condition (ii) by requiring only that those derivatives be known to be $O(1)$ at one point; then the interval of validity of (3.19) is not known *a priori*, except that it is $\geqslant O(1)$ in the rescaled variable. The reason for this is that the higher derivatives are $O(1)$ in the scaling layer, so that it would take an increment in $\hat{y} \geqslant O(1)$ for the terms in (3.19) to deviate from being $O(1)$. Therefore the width of the layer must be at least that large. In the present example, $\mathrm{d}^2\hat{T}/(\mathrm{d}\hat{y})^2 = O(1)$, as indicated above. These criteria for establishing a scaling layer constitute an important ingredient of our analysis, and, significantly, are exactly the same criteria used to establish the valid domains for the classical inner/outer scales.

3.1.4. *Merging layers III and IV*

There is a transparent matching of T^+ as we proceed into layer IV. In fact in view of (3.10),

$$\mathrm{d}\eta = \epsilon^2\mathrm{d}y^+ = \epsilon\mathrm{d}\hat{y}, \quad \mathrm{d}T^+ = \epsilon\mathrm{d}\hat{T},$$

so that

$$\frac{d\hat{T}}{d\hat{y}} = \frac{dT^+}{d\eta}.$$ (3.26)

The middle term in (3.19) is therefore the same as the first in (3.4) and (3.8). Thus, under the simple assumption that $d^2U^+/d\hat{y}^2 \to 0$ as $\hat{y} \to \infty$, the meso equation (3.19) will approach the outer equation (3.8). This says that the derivatives of T^+ match automatically as one passes from layer III to IV.

The behaviour of U^+ is a more complex issue. So far, the only relevant assumption is (3.1). Note that (3.1) was written in terms of the variable y^+, but it holds also for $\hat{y}$ and η. The simplest way to model the behaviour (3.1) (in the variable $\hat{y}$) is by a power law, say $U^+(\hat{y}) \approx A\,\hat{y}^\alpha + B$ as $\hat{y} \to \infty$. The requirements (3.1) compel $0 < \alpha < 1$. Another possibility is a log law: $U^+(\hat{y}) \approx A \ln \hat{y} + B$ as $\hat{y} \to \infty$. Arguments have been made in the past to support one or the other of these forms; these arguments will not be reviewed here.

The boundary condition (3.5), however, dictates that some modification be made near $\eta = 1$ (i.e. in the wake region). This should be done so that U^+ is smooth and even about the centreline. There are many possibilities. These will not be explored herein.

3.2. *Increments in U^+*

In layers I and II, dU^+/dy^+ starts off with the value 1 at $y^+ = 0$ and, according to (3.25), decreases to $O(\epsilon)$ at $y^+ = O(1/\epsilon)$,

$$\left.\frac{dU^+}{dy^+}\right|_{y^+=1/\epsilon} = O(\epsilon).$$ (3.27)

Given this, important questions are: what might be the rate of this decrease, and how does the rate effect the value of U^+ at $y^+ = O(1/\epsilon)$ and the increment $\Delta_{II}U^+$ across layer II? It is natural to propose that dU^+/dy^+ decays according to a power law for large y^+, as in (3.14). The requirement (3.27) says that $C = O(\epsilon^{1-m})$, so set $C = C'\epsilon^{1-m}$. Among these power laws, the simplest is when $m = 1$, so that

$$\frac{dU^+}{dy^+} \approx \frac{C}{y^+};$$ (3.28)

in fact this is the only case in which there is no ϵ-dependence on the right. This case results in a logarithmic law for sufficiently large values of y^+ in layer II:

$$U^+(y^+) \approx C \ln y^+ + D.$$ (3.29)

The associated velocity increment is given by

$$\Delta_{II}U^+ \approx U^+(1/\epsilon) \approx C|\ln \epsilon| + D,$$ (3.30)

which is unbounded as $\epsilon \to 0$.

Another point is that the choice $m = 1$ coincides with the assumption that the law of the wall, i.e. that U^+ depends (to lowest order as $\epsilon \to 0$) only on y^+, holds not only for $y^+ = O(1)$, but also for a range of values of y^+ larger than $O(1)$, namely for $y^+ \leqslant O(1/\epsilon)$. This kind of assumption would be reminiscent of, but not the same as, the classical overlap assumption. More importantly, the possibility of $m \neq 1$ can also be tested, but integration yields the conclusion that if $m \neq 1$, $\Delta_{II}U^+$ is bounded independently of ϵ. This contradicts the velocity increment data which indicate that $\Delta_{II}U/U_c \cong 0.5$, independent of δ^+. Thus only in the logarithmic case does U^+ grow

unboundedly at the end of layer II as $\epsilon \to 0$. Therefore, several arguments can be given to support the claim that (3.29) is valid for large y^+. Work in progress (Fife *et al.*, 2004) points to the existence of a hierarchy of scalings appropriate to the transition zone from II to III; in turn, this hierarchy implies (3.29) and provides still another strong argument in favour of it.

Analogous considerations may apply in part to the transition from III to IV and the increment $\Delta_{IV} U^+$, although that situation is much less clear, as was brought out in §3.1.4. One replaces y^+ by $\hat{y}$. In this case, however, one does not set $dU^+/d\hat{y} = O(\epsilon)$ at the end of the zone, and as a result the velocity increment in this transition process always grows as $\epsilon \to 0$. This, of course, is in accord with the experimental observations. Furthermore, the deviation from a logarithmic-like dependence in the wake region can be excluded from the transition zone; doing so does not effect the unbounded behaviour of $\Delta_{IV} U^+$ as $\epsilon \to 0$. Given that dU^+/dy^+ decays asymptotically according to a power law (while not necessarily exactly equal to a power function), the requirement that this latter increment, divided by $\Delta_{II} U^+$, be $O(1)$ (as prescribed by the experimental data), demands a logarithmic dependence in the mean profile both in the upper part of layer II (transition zone to layer III) and in the lower part of layer IV (transition from layer III).

4. Discussion

The results presented herein have a number of physical and theoretical implications, some of which are now discussed.

4.1. *Physical implications*

A picture of boundary layer structure is revealed that provides a different perspective to the predominant view held in the literature, e.g. Townsend (1976), Monin & Yaglom (1971), Hinze (1975), Tennekes & Lumley (1972), Panton (1990, 1997, 2003), Pope (2000). That is, the traditional view of turbulent wall layer structure is that viscous forces are significant only in the near-wall region (i.e. buffer layer and below), see Gad-el-Hak & Bandyopadhyay (1994). Outside of this near-wall region it is assumed that viscous forces play a negligible role. This is believed to underlie the Reynolds number similarity for the law of the wall, as well as the characterization of the logarithmic layer as an inertial sublayer in physical space (e.g. Tennekes & Lumley 1972). From this, turbulent wall layers are usually divided into the four regions of the mean velocity profile, i.e. the viscous sublayer, buffer layer, log-layer and wake layer mentioned in the Introduction.

The traditional picture is primarily supported by the properties of the stress field and the mean velocity profile. As is widely known, the viscous stress is high very near the wall. At $y^+ \cong 10$, however, the viscous and Reynolds stress are approximately equal, and by $y^+ \cong 30$ the viscous stress is only about 10% of the Reynolds stress. Farther from the wall the viscous stress becomes an even smaller fraction. However, it is the gradients of these stresses that are the relevant dynamical quantities. Considering this, the traditional interpretation of turbulent wall flows is deemed inappropriate for educing the correct time-averaged dynamics.

The present results indicate that the inner viscous/pressure gradient layer structure in channels is different from the inner viscous/advection layer in boundary layers. That is, at the channel wall the viscous stress gradient balances the pressure gradient (so it is not the only significant term in the momentum balance equation), and there is an associated flux of vorticity from the surface. In the zero-pressure-gradient

boundary layer, however, all of the terms in the mean momentum equation are zero at the wall, and there is no net flux of vorticity. The influence of these differences can be seen by expanding the near-wall region of the stress-gradient ratio profiles in figures 1 and 3. When this is done, it becomes apparent that in the channel the viscous/advection layer is thicker at low Reynolds number, and that the ratio of -1 in the stress gradient balance layer is approached asymptotically, probably owing to the net diminishing effect of the diffusive surface flux of vorticity. In the boundary layer, however, the value of this ratio is apparently -1 even at very low Reynolds number.

Also significant are modifications to the interpretation of logarithmic layer structure. As mentioned previously, the commonly held interpretation of the logarithmic layer as constituting an inertial subrange in physical space requires revision. That is, since viscous effects are significant in both the stress-gradient balance layer and the meso viscous/advection layer, only the outer portion of the logarithmic layer (i.e. the portion that adjoins the inertial/advection layer) might rationally be considered an inertial sublayer. Given this, characteristics of logarithmic layer turbulence are also likely to change depending on the force balance layer from which it is sampled. The present results also provide evidence that characterization of the logarithmic layer as a simple overlap layer is inappropriate. In connection with this it is instructive to note the recent observations of Osterlund *et al.* (1999). Specifically, while they assert that there is no significant Reynolds number dependence for the classical logarithmic relation, they do point out that a viscous influence exists in an extended 'buffer region' to $y^+ \cong 200$, instead of the more traditionally held value of $y^+ \cong 50$. Their experiments, however, ranged from $Re_\theta = 2500$ to 27000. Given this, the present results indicate that the stress-gradient balance layer extends to about $y^+ \cong 40$ followed by a meso viscous/advection layer extending to about $y^+ \cong 66$ for their lowest Reynolds number. For their highest Reynolds number, $Re_\theta \cong 27000$, the stress-gradient balance layer extends to about $y^+ \cong 120$ followed by the meso viscous/advection layer out to about $y^+ \cong 203$. Similar empirically based conjectures have been made regarding the existence of two distinct logarithmic/power law-like scaling regions in pipe and channel flow, Zagarola & Smits (1998), Wosnik *et al.* (2000) and Afzal (2001*a*, *b*). The present results provide a physical explanation for these observations.

Across the meso viscous/advection layer the Reynolds stress gradient changes sign. This indicates that turbulent inertia shifts from a net momentum source for $y < y_m$ to a net momentum sink for $y > y_m$. For this reason, it is likely that the significant inner/outer interactions occur across the meso viscous/advection layer. Similarly, the re-emergence of mean advection effects in the inner viscous/advection layer are probably associated with the recent observations of Metzger & Klewicki (2001) indicating that low-frequency motions are prevalent at high Reynolds number even very near the wall, as well as the successful scaling of the near-wall axial stress using the mixed velocity scale, $\sqrt{U_\infty u_\tau}$, as found by DeGraaff & Eaton (2000).

Regarding flow physics, it is also worth noting that the present findings hold considerable promise in classifying and/or characterizing non-canonical boundary layer flows. That is, non-equilibrium effects (associated with, for example, pressure gradients and/or added strain rates) are likely to be clearly reflected in deviations from the force balance layer structure depicted herein. Similarly, since surface roughness imposes external length scales within the flow, the relation between these imposed scales and the thickness of the stress-gradient balance layer thickness is likely to be a significant measure of roughness influences, as well as the Reynolds number dependence of roughness effects.

4.2. *Theoretical implications*

Unlike more familiar multiscale analyses, the present one is not amenable to a full-blown matched asymptotics approch, such as where matching conditions lead to boundary conditions at ∞ or at 0, and are used to determine inner and outer solutions uniquely. The differential equations in this case are underdetermined, and thus cannot be used to obtain a unique solution for the mean velocity. Nevertheless, considerable qualitative information about these unknown solutions was extracted. Since this information directly reflects the behaviour of the mean momentum balance, it is felt to be particularly useful in assessing the viability of proposed analytical/approximate formulae for the mean velocity profile. That is, the mathematical properties derived herein comprise a set of criteria that any candidate mean velocity profile equation (e.g. once inserted in the mean momentum balance) must satisfy. In connection with this, it is important to note that at least some of these criteria are rather robust relative to the inherent capabilities of experimental data. For example, the analysis in §3.2 indicated that effectively distinguishing between a power or logarithmic form for the mean profile required determining whether $\Delta_{II}U^+$ remained $O(1)$ or underwent an unbounded increase with increasing Reynolds number. Such a distinction is considerably more attainable with experimental measurements than via use of the $y^+(\mathrm{d}U^+/\mathrm{d}y^+)$ and $(y^+/U^+)(\mathrm{d}U^+/\mathrm{d}y^+)$ indicator functions mentioned in the Introduction.

The present analysis provides a theoretical justification for the intermediate boundary layer length scale empirically identified via examination of the stress gradient ratios. This intermediate meso-scale, $l_m = \sqrt{\nu\delta/u_\tau}$, follows directly from the layer III rescaling given in §3.1.2. Note that this rescaling was formally derived and is required to render all the terms in the mean momentum balance formally of the same magnitude in layer III. Simply stated, l_m has the same theoretical relevance as either the inner scale, $l_i = \nu/u_\tau$, or the outer scale, $l_o = \delta$. Note further that normalization of wall-normal distance by l_m yields $\sqrt{y^2}/\sqrt{\nu\delta/u_\tau} = \sqrt{\eta y^+}$. This is both $\hat{y}$ (as measured relative to y_m) and the geometric mean of the inner and outer normalized distance from the wall. Regarding the former, it is apparent that given any two of the three length scales, the third may be determined. Regarding the latter, it would seem that geometric mean (intermediate or mixed) scalings, often empirically identified as being superior to either inner or outer scalings (Alfredsson & Johansson 1984; Afzal 1984b; Klewicki & Falco 1996; DeGraaff & Eaton 2000; Priyadarshana & Klewicki 2003; Metzger, Klewicki & Priyadarshana 2003), but just as often discounted owing to their purported lack of physical significance or theoretical justification, e.g. Gad-el-Hak & Bandyopadhyay (1994), are worthy of continuing investigation.

Finally, the current work provides a unifying context for several previous boundary layer observations and analyses that have identified 'intermediate' (Afzal 1982; Sahay 1997), 'critical' (Sreenivasan & Sahay 1997), and 'meso'-layers (Long & Chen 1981). Each of these identify an important region around the peak in the Reynolds stress that scales with mixed variables. The analysis and empirical observations of Sahay (1997) and Sreenivasan & Sahay (1997) focused on the ratio of the viscous stress gradient to Reynolds stress gradient in the vicinity of the peak in the Reynolds stress, with an emphasis of the importance of viscous effects in this region. Afzal (1982) developed a scaling for an intermediate layer around the peak in the Reynolds stress (which he subsequently used to match with both the inner and outer layer using classical overlap ideas) by assuming all terms in the 'once-integrated' momentum equation are of the same order in this region. This resulted in the intermediate scalings developed here in §3.1.2. In each of these works, the intermediate layer identified is essentially

the meso-layer (layer III) discussed in this work with its dynamical relevance revealed by examination of the stress gradient data in figures 1–3 herein. The present work expands upon these earlier works by revealing (i) the existence of the stress-gradient balance region (layer II), in which viscous effects are important at all y^+ up to a point beyond the peak in the Reynolds stress (and not simply in the vicinity of this peak), and (ii) the mathematical requirement for the intermediate length to adequately describe the scaling behaviour of the mean momentum balance.

5. Conclusions

The time-mean differential momentum equation for canonical turbulent wall flows indicates that stress gradients are the appropriate quantities to examine for educing dynamics. Given this, available premier-quality experimental data and DNS simulations were used to reveal the properties and Reynolds-number dependence of the mean structure of boundary layer, pipe and channel flows. A four-layer structure of these canonical wall flows was revealed. The dynamical structure of each layer was described and the Reynolds-number dependent properties of the thickness and circulation of each layer quantified. From this analysis, a Reynolds-number-dependent intermediate length scale for turbulent wall flows was identified. This length scale arises directly from the internal dynamics and characterizes the thickness of the viscous–inertial stress-gradient balance layer. The present view of wall flow structure is in contrast to the established and pervasive view. The present picture of mean dynamics is directly founded on the mean statement of Newton's second law for turbulent wall layers.

To complement these empirical observations, a multiscale analysis of the properties of the mean momentum balance in statistically stationary, fully developed, turbulent channel flow has been developed. The analysis employed minimal assumptions beyond the averaged momentum equation itself, an example being that the mean velocity monotonically increases from the wall to the channel centreline. With this, all properties and Reynolds-number scalings shown empirically were derived in a systematic manner. Three different scalings (inner, outer and meso) were shown to be relevant, each in their own region, with the regions characterized by Reynolds-number dependent intervals of distance from the wall. Specific mathematical properties and scaling behaviour of the mean streamwise velocity, Reynolds stress and their wall-normal gradients were derived for each of the domains, and, in each case, were shown to be in full agreement with channel flow DNS and Princeton Superpipe data. These properties include the physical extent and Reynolds-number dependent scaling of the layer thicknesses, a flattening of the Reynolds stress profile near its maximum, the mean velocity increment across each layer, the rate of decay of the mean velocity gradient (especially in the stress-gradient balance layer), the asymptotic rate of increase of the peak value of the Reynolds stress, as well as compelling evidence for the logarithmic character of the mean profile in two distinct regions of the flow.

REFERENCES

AFZAL, N. 1976 Millikan's argument at moderately large Reynolds number. *Phys. Fluids* **19**, 600–602.

AFZAL, N. 1982 Fully developed turbulent flow in a pipe: an intermediate layer. *Ing.-Arch.* **52**, 355–377.

AFZAL, N. 1984*a* Mesolayer theory for turbulent flows. *AIAA J.* **22**, 437–439.

AFZAL, N. 1984*b* Periods between bursting in turbulent shear flow: Intermediate layer. *Current Science* **53**, 640–642.

AFZAL, N. 2001*a* Power law and log law velocity profiles in fully developed turbulent boundary layer flow: equivalent relations at large Reynolds number. *Acta Mechanica* **151**, 195–216.

AFZAL, N. 2001*b* Power law and log law velocity profiles in fully developed turbulent pipe flow: equivalent relations at large Reynolds number. *Acta Mechanica* **151**, 171–183.

ALFREDSSON, P. H. & JOHANSSON, A. V. 1984 Time scales in turbulent channel flow. *Phys. Fluids* **27**, 1974–1981.

BARENBLATT, G. I., CHORIN, A. & PROSTOKISHIN, V. M. 1997 Scaling laws for fully developed flow in pipes. *Appl. Mech. Rev.* **50**, 413–429.

BUSCHMANN, M. H. & GAD-EL-HAK, M. 2003 Debate concerning the mean-velocity profile of a turbulent boundary layer. *AIAA J.* **41**, 565–572.

CENEDESE, A., ROMANO, G. P. & ANTONIA, R. A. 1998 A comment on the "linear" law of the wall for fully developed turbulent channel flow. *Exps. Fluids* **25**, 165–170.

DEGRAAFF, D. B. & EATON, J. K. 2000 Reynolds-number scaling of the flat-plate turbulent boundary layer. *J. Fluid Mech.* **422**, 319–346.

FIFE, P., WEI, T., KLEWICKI, J. & MCMURTRY, P. 2004 Stress gradient balance layers and scale hierarchies in wall-bounded turbulent flows. *J. Fluid Mech.* (submitted).

GAD-EL-HAK, M. & BANDYOPADHYAY, P. R. 1994 Reynolds number effects in wall-bounded turbulent flows. *Appl. Mech. Rev.* **47**, 307–365.

GEORGE, W. K. & CASTILLO, L. 1997 Zero-pressure-gradient turbulent boundary layer. *Appl. Mech. Rev.* **50**, 689–729.

GILL, A. E. 1968 The Reynolds number similarity argument. *J. Maths Phys.* **47**, 437–441.

HINZE, J. O. 1975 *Turbulence*, 2nd Edn. McGraw-Hill.

IZAKSON, A. 1937 On the formula for the velocity distribution near walls. *Tech. Phys. USSR* **IV**, **2**, 155–162.

KEVORKIAN, J. & COLE, J. D. 1981 *Perturbation Methods in Applied Mathematics*. Springer.

KLEWICKI, J. C. 1989 On the interactions between the inner and outer region motions in turbulent boundary layers. PhD thesis, Michigan State University.

KLEWICKI, J. C. & FALCO, R. E. 1996 Spanwise vorticity structure in turbulent boundary layer. *Intl J. Heat Fluid Flow* **17**, 363–376.

LIGHTHILL, M. J. 1963 *Laminar Boundary Layers* (ed. L. Rosenhead), chap. ii. Clarendon.

LONG, R. R. & CHEN, T.-C. 1981 Experimental evidence for the existence of the mesolayer in turbulent systems. *J. Fluid Mech.* **105**, 19–59.

MCKEON, B. J., LI, J., JIANG, W., MORRISON, J. F. & SMITS, A. J. 2003 Pitot probe corrections in fully developed turbulent pipe flow. *Meas. Sci. Tech.* **14**, 1449–1458.

METZGER, M. M. & KLEWICKI, J. C. 2001 A comparative study of near–wall turbulence in high and low Reynolds number boundary layers. *Phys. Fluids* **13**, 692–701.

METZGER, M. M., KLEWICKI, J. C. & PRIYADARSHANA, P. A. 2003 Reynolds number dependence in the behavior of boundary layer axial stress and scalar variance transport. In *Reynolds Number Scaling in Turbulent Flow* (ed. A. J. Smits), pp. 83–88. Kluwer.

MILLIKAN, C. B. 1939 A critical discussion of turbulent flows in channel and circular tubes. In *Proc. Fifth Intl Congr. of Applied Mechanics* (ed. J. P. D. Hartog & H. Peters), pp. 386–392. Wiley.

MONIN, A. S. & YAGLOM, A. M. 1971 *Statistical Fluid Mechanics*, 1st Edn. MIT Press.

MOSER, R. D., KIM, J. & MANSOUR, N. N. 1999 Direct numerical simulation of turbulent channel flow up to $Re_\tau = 590$. *Phys. Fluids* **11**, 943–945.

OSTERLUND, J. M., JOHANSSON, A. V., NAGIB, H. M. & HITES, M. H. 1999 Wall shear stress measurements in high Reynolds number boundary layers from two facilities. In *30th AIAA Fluid Dynamics Conf., Norfolk, VA*.

PANTON, R. L. 1990 Scaling turbulent wall layers. *Trans. ASME: J. Fluids Engng* **112**, 425–432.

PANTON, R. L. 1997 A Reynolds stress function for wall layers. *Trans. ASME: J. Fluids Engng* **119**, 325–330.

PANTON, R. L. 2002 Evaluation of the Barenblatt-Chorin-Prostokishin power law for turbulent boundary layers. *Phys. Fluids* **14**, 1806–1808.

PANTON, R. L. 2003 Wall turbulence described by composite expansions. Preprint.

PERRY, A. E., HAFEZ, S. & CHONG, M. S. 2001 A possible reinterpretation of the Princeton superpipe data. *J. Fluid Mech.* **439**, 395–401.

POPE, S. B. 2000 *Turbulent Flow*, 1st Edn. Cambridge University Press.

PRIYADARSHANA, P. A. & KLEWICKI, J. C. 2003 Reynolds number scaling of wall layer velocity-vorticity products. In *Reynolds Number Scaling in Turbulent Flow* (ed. A. J. Smits), pp. 117–122. Kluwer.

SAHAY, A. 1997 The mean velocity and the Reynolds shear stress in turbulent channel and pipe flow. PhD thesis, Yale University, http://wwwlib.umi.com/dissertations.

SPALART, P. R. 1988 Direct simulation of a turbulent boundary layer up to $Re_\theta = 1410$. *J. Fluid Mech.* **187**, 61–98.

SREENIVASAN, K. R. & SAHAY, A. 1997 The persistence of viscous effects in the overlap region, and the mean velocity in turbulent pipe and channel flows. In *Self-Sustaining Mechanisms of Wall Turbulence* (ed. R. Panton), pp. 253–272. Computational Mechanics Publications, Southampton, UK.

TENNEKES, H. & LUMLEY, J. L. 1972 *First Course in Turbulence*, 1st Edn. MIT Press.

TOWNSEND, A. A. 1976 *The Structure of Turbulent Shear Flow*, 2nd Edn. Cambridge University Press.

WILLMARTH, W. W. 1975 Structure of turbulence in boundary layers. *Adv. Appl. Mech.* **15**, 159–254.

WOSNIK, M., CASTILLO, L. & GEORGE, W. K. 2000 A theory for turbulent pipe and channel flow. *J. Fluid Mech.* **421**, 115–145.

ZAGAROLA, M. V. & SMITS, A. J. 1997 Scaling of the mean velocity profile for turbulent pipe flow. *Phys. Rev. Lett.* **78** (1), 239–242.

ZAGAROLA, M. V. & SMITS, A. J. 1998 Mean-flow scaling of turbulent pipe flow. *J. Fluid Mech.* **373**, 33–79.

ZANOUN, E., NAGIB, H., DURST, F. & MONKEWITZ, P. 2002 Higher Reynolds number channel data and their comparison to recent asymptotic theory (Invited). *AIAA Paper* 2002–1102.